11

AC and DC Equivalent Circuit Modeling of the Discontinuous Conduction Mode

So far, we have derived equivalent circuit models for dc–dc pulse-width modulation (PWM) converters operating in the continuous conduction mode. As illustrated in Fig. 11.1, the basic dc conversion property is modeled by an effective dc transformer, having a turns ratio equal to the conversion ratio $M(D)$. This model predicts that the converter has a voltage-source output characteristic, such that the output voltage is essentially independent of the load current or load resistance R. We have also seen how to refine this model, to predict losses and efficiency, converter dynamics, and small-signal ac transfer functions. We found that the transfer functions of the buck converter contain two low-frequency poles, owing to the converter filter inductor and capacitor. The control-to-output transfer functions of the boost and buck-boost converters additionally contain a right half-plane zero. Finally, we have seen how to utilize these results in the design of converter control systems.

What are the basic dc and small-signal ac equivalent circuits of converters operating in the discontinuous conduction mode (DCM)? It was found in Chapter 5 that, in DCM, the output voltage becomes load-dependent: the conversion ratio $M(D, K)$ is a function of the dimensionless parameter $K = 2L/RT_s$, which in turn is a function of the load resistance R. So the converter no longer has a voltage-source output characteristic, and hence the dc transformer model is less appropriate. In this chapter, the averaged switch modeling [1-8] approach is employed, to derive equivalent circuits of the DCM switch network.

In Section 11.1, it is shown that the *loss-free resistor* model [9-11] is the averaged switch model of the DCM switch network. This equivalent circuit represents the steady-state and large-signal dynamic characteristics of the DCM switch network, in a clear and simple manner. In the discontinuous conduction mode, the average transistor voltage and current obey Ohm's law, and hence the transistor is modeled by an effective resistor R_e. The average diode voltage and current obey a power source characteristic, with power equal to the power effectively dissipated in R_e. Therefore, the diode is modeled with a *dependent power source.*

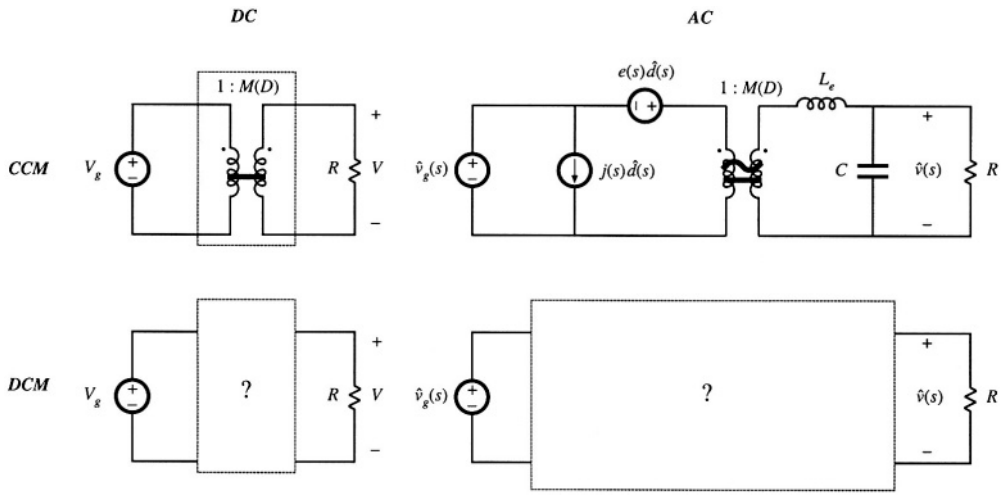

Fig. 11.1 The objective of this chapter is the derivation of large-signal dc and small-signal ac equivalent circuit models for converters operating in the discontinuous conduction mode.

Since most converters operate in discontinuous conduction mode at some operating points, small-signal ac DCM models are needed, to prove that the control systems of such converters are correctly designed. In Section 11.2, a small-signal model of the DCM switch network is derived by linearization of the loss-free resistor model. The transfer functions of DCM converters are quite different from their respective CCM transfer functions. The basic DCM buck, boost, and buck-boost converters essentially exhibit simple single-pole transfer functions [12, 13], in which the second pole and the RHP zero (in the case of boost and buck-boost converters) are at high frequencies. So the basic converters operating in DCM are easy to control; for this reason, converters are sometimes purposely operated in DCM for all loads. The transfer functions of higher order converters such as the DCM Ćuk or SEPIC are considerably more complicated; but again, one pole is shifted to high frequency, where it has negligible practical effect. This chapter concludes, in Section 11.3, with a discussion of a more detailed analysis used to predict high-frequency dynamics of DCM converters. The more detailed analysis predicts that the high-frequency pole of DCM converters occurs at frequencies near or exceeding the switching frequency [2-6]. The RHP zero, in the case of DCM buck-boost and boost converters, also occurs at high frequencies. This is why, in practice, the high-frequency dynamics can usually be neglected in DCM.

11.1 DCM AVERAGED SWITCH MODEL

Consider the buck-boost converter of Fig. 11.2. Let us follow the averaged switch modeling approach of Section 7.4, to derive an equivalent circuit that models the averaged terminal waveforms of the switch network. The general two-switch network and its terminalquantities $v_1(t)$, $i_1(t)$, $v_2(t)$, and $i_2(t)$ are defined as illustrated in Fig. 11.2, consistent with Fig. 7.39(a). The inductor and switch network voltage and current waveforms are illustrated in Fig. 11.3, for DCM operation.

The inductor current is equal to zero at the beginning of each switching period. During the first subinterval, while the transistor conducts, the inductor current increases with a slope of $v_g(t)/L$. At the

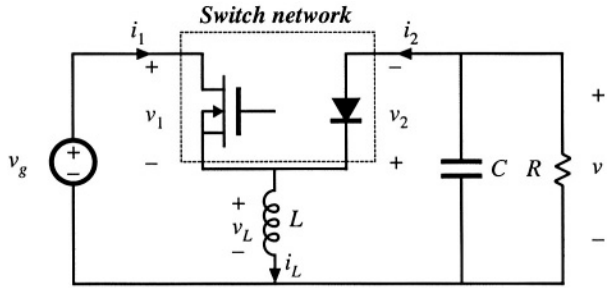

Fig. 11.2 Buck-boost converter example, with switch network terminal quantities identified.

end of the first subinterval, the inductor current $i_L(t)$ attains the peak value given by

$$i_{pk} = \frac{v_g}{L} d_1 T_s \tag{11.1}$$

During the second subinterval, while the diode conducts, the inductor current decreases with a slope equal to $v(t)/L$. The second subinterval ends when the diode becomes reverse-biased, at time $t = (d_1 + d_2)T_s$. The inductor current then remains at zero for the balance of the switching period. The inductor voltage is zero during the third subinterval.

A DCM averaged switch model can be derived with reference to the waveforms of Fig. 11.3. Following the approach of Section 7.4.2, let us find the average values of the switch network terminal waveforms $v_1(t)$, $v_2(t)$, $i_1(t)$, and $i_2(t)$ in terms of the converter state variables (inductor currents and capacitor voltages), the input voltage $v_g(t)$, and the subinterval lengths d_1 and d_2.

The average switch network input voltage $\langle v_1(t) \rangle_{T_s}$, or the average transistor voltage, is found by averaging the $v_1(t)$ waveform of Fig. 11.3:

$$\langle v_1(t) \rangle_{T_s} = d_1(t) \cdot 0 + d_2(t) \left(\langle v_g(t) \rangle_{T_s} - \langle v(t) \rangle_{T_s} \right) + d_3(t) \langle v_g(t) \rangle_{T_s} \tag{11.2}$$

Use of the identity $d_3(t) = 1 - d_1(t) - d_2(t)$ yields

$$\langle v_1(t) \rangle_{T_s} = \left(1 - d_1(t)\right) \langle v_g(t) \rangle_{T_s} - d_2(t) \langle v(t) \rangle_{T_s} \tag{11.3}$$

Similar analysis leads to the following expression for the average diode voltage:

$$\begin{aligned} \langle v_2(t) \rangle_{T_s} &= d_1(t) \left(\langle v_g(t) \rangle_{T_s} - \langle v(t) \rangle_{T_s} \right) + d_2(t) \cdot 0 + d_3(t) \left(- \langle v(t) \rangle_{T_s} \right) \\ &= d_1(t) \langle v_g(t) \rangle_{T_s} - \left(1 - d_2(t)\right) \langle v(t) \rangle_{T_s} \end{aligned} \tag{11.4}$$

The average switch network input current $\langle i_1(t) \rangle_{T_s}$ is found by integrating the $i_1(t)$ waveform of Fig. 11.3 over one switching period:

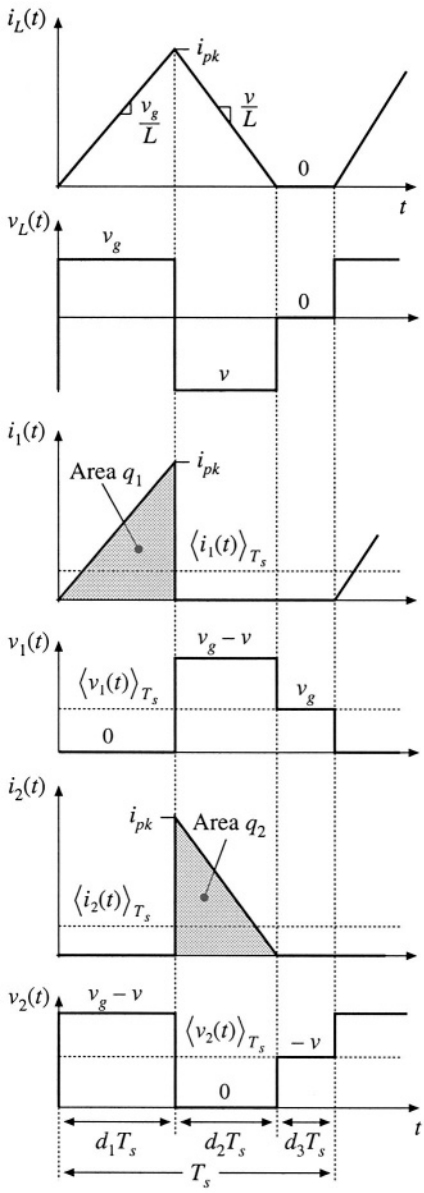

Fig. 11.3 Inductor and switch network voltage and current waveforms.

$$\langle i_1(t)\rangle_{T_s} = \frac{1}{T_s}\int_t^{t+T_s} i_1(t)dt = \frac{q_1}{T_s} \tag{11.5}$$

The integral q_1 is equal to the area under the $i_1(t)$ waveform during the first subinterval. This area is easily evaluated using the triangle area formula:

$$q_1 = \int_t^{t+T_s} i_1(t)dt = \frac{1}{2}\left(d_1T_s\right)\left(i_{pk}\right) \tag{11.6}$$

Substitution of Eqs. (11.1) and (11.6) into Eq. (11.5) gives:

$$\langle i_1(t)\rangle_{T_s} = \frac{d_1^2(t)T_s}{2L}\langle v_g(t)\rangle_{T_s} \tag{11.7}$$

Note that $\langle i_1(t)\rangle_{T_s}$ is not equal to $d_1\langle i_L(t)\rangle_{T_s}$. Since the inductor current ripple is not small, it is necessary to sketch the actual input current waveform, including the large switching ripple, and then correctly compute the average as in Eqs. (11.5) to (11.7).

The average diode current $\langle i_2(t)\rangle_{T_s}$ is found in a manner similar to that used above for $\langle i_1(t)\rangle_{T_s}$:

$$\langle i_2(t)\rangle_{T_s} = \frac{1}{T_s}\int_t^{t+T_s} i_2(t)dt = \frac{q_2}{T_s} \tag{11.8}$$

The integral q_2 is equal to the area under the $i_2(t)$ waveform during the second subinterval. This area is evaluated using the triangle area formula:

$$q_2 = \int_t^{t+T_s} i_2(t)dt = \frac{1}{2}\left(d_2T_s\right)\left(i_{pk}\right) \tag{11.9}$$

Substitution of Eqs. (11.1) and (11.9) into Eq. (11.8) leads to:

$$\langle i_2(t)\rangle_{T_s} = \frac{d_1(t)d_2(t)T_s}{2L}\langle v_g(t)\rangle_{T_s} \tag{11.10}$$

Equations (11.3), (11.4), (11.7) and (11.10) constitute the averaged terminal equations of the switch network in the DCM buck-boost converter. In these equations, it remains to express the subinterval length d_2 in terms of the switch duty cycle $d_1 = d$, and the converter averaged waveforms. One approach to finding the subinterval length d_2 is by solving the inductor current waveform. In the buck-boost converter, the diode switches off when the inductor current reaches zero, at the end of the sec-

ond subinterval. As a result, $i_L(T_s) = i_L(0) = 0$. There is no net change in inductor current over one complete switching period, and no net volt-seconds are applied to the inductor over any complete switching period that starts at the time when the transistor is turned on. Therefore, the average inductor voltage computed over this period is zero,

$$\langle v_L(t)\rangle_{T_s} = d_1\langle v_g(t)\rangle_{T_s} + d_2\langle v(t)\rangle_{T_s} + d_3 \cdot 0 = 0 \tag{11.11}$$

even when the converter is not in equilibrium. This equation can be used to find the length of the second subinterval:

$$d_2(t) = -d_1(t)\frac{\langle v_g(t)\rangle_{T_s}}{\langle v(t)\rangle_{T_s}} \tag{11.12}$$

Substitution of Eq. (11.12) into Eqs. (11.3), (11.4), (11.7) and (11.10), allows us to obtain simple expressions for the averaged terminal waveforms of the switch network in the discontinuous conduction mode:

$$\langle v_1(t)\rangle_{T_s} = \langle v_g(t)\rangle_{T_s} \tag{11.13}$$

$$\langle v_2(t)\rangle_{T_s} = -\langle v(t)\rangle_{T_s} \tag{11.14}$$

$$\langle i_1(t)\rangle_{T_s} = \frac{d_1^2(t)T_s}{2L}\langle v_1(t)\rangle_{T_s} \tag{11.15}$$

$$\langle i_2(t)\rangle_{T_s} = \frac{d_1^2(t)T_s}{2L}\frac{\langle v_1(t)\rangle_{T_s}^2}{\langle v_2(t)\rangle_{T_s}} \tag{11.16}$$

Let us next construct an equivalent circuit corresponding to the averaged switch network equations (11.15) and (11.16). The switch network input port is modeled by Eq. (11.15). This equation states that the average input current $\langle i_1(t)\rangle_{T_s}$ is proportional to the applied input voltage $\langle v_1(t)\rangle_{T_s}$. In other words, the low-frequency components of the switch network input port obey Ohm's law:

$$\langle i_1(t)\rangle_{T_s} = \frac{\langle v_1(t)\rangle_{T_s}}{R_e(d_1)} \tag{11.17}$$

where the effective resistance R_e is

$$R_e(d_1) = \frac{2L}{d_1^2 T_s} \tag{11.18}$$

An equivalent circuit is illustrated in Fig. 11.4. During the first subinterval, the slope of the input current waveform $i_1(t)$ is proportional to the input voltage $\langle v_g(t)\rangle_{T_s} = \langle v_1(t)\rangle_{T_s}$, as illustrated in Fig. 11.3. As a result, the peak current i_{pk}, the total charge q_1, and the average input current $\langle i_1(t)\rangle_{T_s}$, are also proportional to $\langle v_1(t)\rangle_{T_s}$. Of course, there is no physical resistor inside the converter. Indeed, if the converter elements are ideal, then no heat is generated inside the converter. Rather, the power apparently consumed by R_e is transferred to the switch network output port.

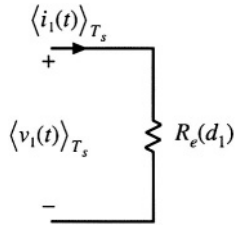

Fig. 11.4 Equivalent circuit that models the average waveforms of the switch input (transistor) port.

The switch network output (diode) port is modeled by Eq. (11.16), or

$$\langle i_2(t)\rangle_{T_s}\langle v_2(t)\rangle_{T_s} = \frac{\langle v_1(t)\rangle^2_{T_s}}{R_e(d_1)} = \langle p(t)\rangle_{T_s} \tag{11.19}$$

Note that $\langle v_1(t)\rangle^2_{T_s}/R_e$ is the average power $\langle p(t)\rangle_{T_s}$ apparently consumed by the effective resistor $R_e(d_1)$. Equation (11.19) states that this power flows out of the switch network output port. So the switch network consumes no net power—its average input and output powers are equal.

Equation (11.19) can also be derived by consideration of the inductor stored energy. During the first subinterval, the inductor current increases from 0 to i_{pk}. In the process, the inductor stores the following energy:

$$\frac{1}{2}Li^2_{pk} = \frac{\langle v_1\rangle^2_{T_s} d_1^2 T_s^2}{2L} = \frac{\langle v_1\rangle^2_{T_s}}{R_e(d_1)} T_s \tag{11.20}$$

Here, i_{pk} has been expressed in terms of $\langle v_1(t)\rangle_{T_s}$ using Eqs. (11.1) and (11.13). This energy is transferred from the source v_g, through the switch network input terminals (i.e., through the transistor), to the inductor. During the second subinterval, the inductor releases all of its stored energy through the switch network output terminals (i.e., through the diode), to the output. The average output power can therefore be expressed as the energy transferred per cycle, divided by the switching period:

$$\langle p(t)\rangle_{T_s} = \left(\frac{\langle v_1\rangle^2_{T_s}}{R_e(d_1)} T_s\right)\left(\frac{1}{T_s}\right) = \frac{\langle v_1\rangle^2_{T_s}}{R_e(d_1)} \tag{11.21}$$

This power is transferred to the load, and hence

$$\langle v\rangle_{T_s}\langle i_2\rangle_{T_s} = \langle v_2\rangle_{T_s}\langle i_2\rangle_{T_s} = \langle p(t)\rangle_{T_s} = \frac{\langle v_1\rangle^2_{T_s}}{R_e(d_1)} \tag{11.22}$$

This result coincides with Eq. (11.19).

The average power $\langle p(t)\rangle_{T_s}$ is independent of the load characteristics, and is determined solely by the effective resistance R_e and the applied switch network input terminal voltage or current. In other words, the switch network output port behaves as a source of power, equal to the power apparently consumed by the effective resistance R_e. This behavior is represented schematically by the dependent power source symbol illustrated in Fig. 11.5. In any lossless two-port network, when the voltage and current at one port are independent of the characteristics of the external network connected to the second port, then the second port must exhibit a dependent power source characteristic [10]. This situation arises in a num-

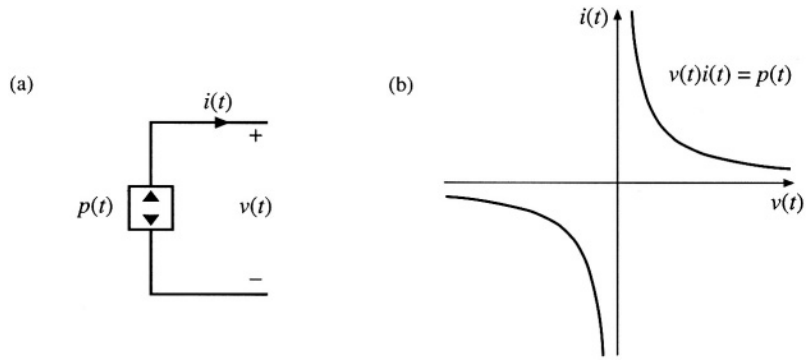

Fig. 11.5 The dependent power source: (a) schematic symbol, (b) i–v characteristic.

ber of common power-processing applications, including switch networks operating in the discontinuous conduction mode.

The power source characteristic illustrated in Fig. 11.5(b) is symmetrical with respect to voltage and current; in consequence, the power source exhibits several unique properties. Similar to the voltage source, the ideal power source must not be short-circuited; otherwise, infinite current occurs. And similar to the current source, the ideal power source must not be open-circuited, to avoid infinite terminal voltage. The power source must be connected to a load capable of absorbing the power $p(t)$, and the operating point is defined by the intersection of the load and power source i–v characteristics.

As illustrated in Fig. 11.6(a), series- and parallel-connected power sources can be combined

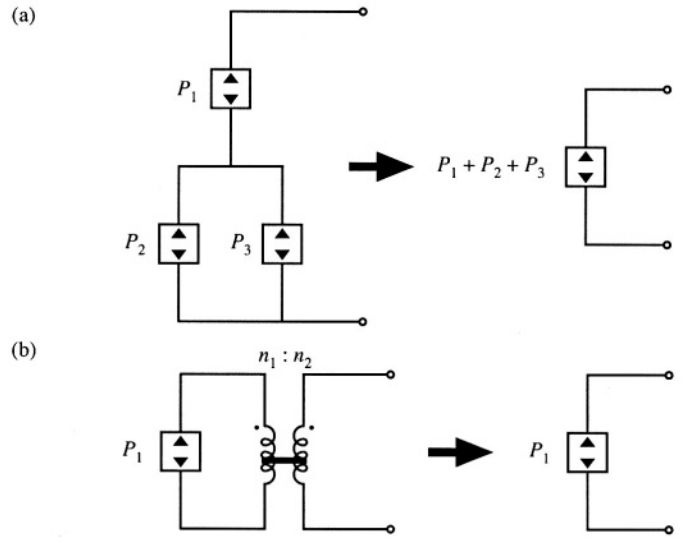

Fig. 11.6 Circuit manipulations of power source elements: (a) combination of series- and parallel- connected power sources into a single equivalent power source, (b) invariance of the power source to reflection through an ideal transformer of arbitrary turns ratio.

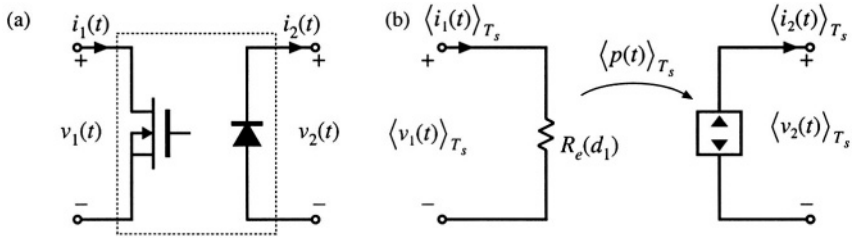

Fig. 11.7 (a) the general two-switch network, and (b) the corresponding averaged switch model in the discontinuous conduction mode: the average transistor waveforms obey Ohm's law, while the average diode waveforms behave as a dependent power source.

into a single power source, equal to the sum of the powers of the individual sources. Fig. 11.6(b) illustrates how reflection of a power source through a transformer, having an arbitrary turns ratio, leaves the power source unchanged. Power sources are also invariant to duality transformations.

The averaged large-signal model of the general two-switch network in DCM is illustrated in Fig. 11.7(b). The input port behaves effectively as resistance R_e. The instantaneous power apparently consumed by R_e is transferred to the output port, and the output port behaves as a dependent power source. This lossless two-port network is called the *loss-free resistor* model (LFR) [9]. The loss-free resistor represents the basic power conversion properties of DCM switch networks [11]. It can be shown that the loss-free resistor models the averaged properties of DCM switch networks not only in the buck-boost converter, but also in other PWM converters.

When the switch network of the DCM buck-boost converter is replaced by the averaged model of Fig. 11.7(b), the converter equivalent circuit of Fig. 11.8 is obtained. Upon setting all averaged waveforms to their quiescent values, and letting the inductor and capacitor become a short-circuit and an open-circuit, respectively, we obtain the dc model of Fig. 11.9.

Systems containing power sources or loss-free resistors can usually be easily solved, by equating average source and load powers. For example, in the dc network of Fig. 11.9, the power flowing into the converter input terminals is

$$P = \frac{V_g^2}{R_e} \tag{11.23}$$

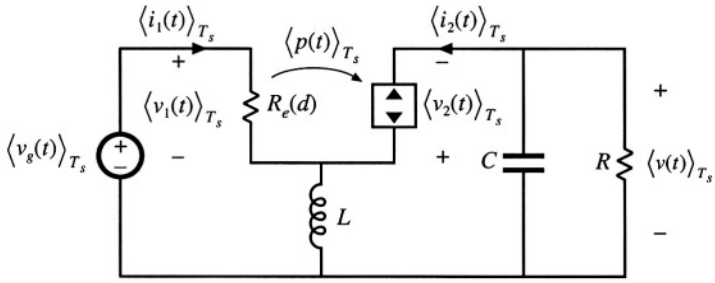

Fig. 11.8 Replacement of the switch network of the DCM buck-boost converter with the loss-free resistor model.

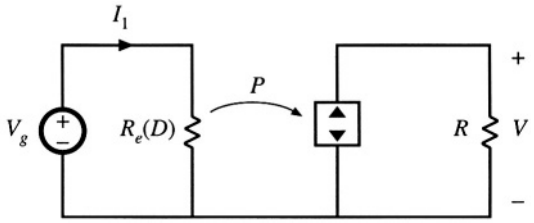

Fig. 11.9 Dc network example containing a loss-free resistor model.

The power flowing into the load resistor is

$$P = \frac{V^2}{R} \tag{11.24}$$

The loss-free resistor model states that these two powers must be equal:

$$P = \frac{V_g^2}{R_e} = \frac{V^2}{R} \tag{11.25}$$

Solution for the voltage conversion ratio $M = V/V_g$ yields

$$\frac{V}{V_g} = \pm\sqrt{\frac{R}{R_e}} \tag{11.26}$$

Equation (11.26) is a general result, valid for any converter that can be modeled by a loss-free resistor and that drives a resistive load. Other arguments must be used to determine the polarity of V/V_g. In the buck-boost converter shown in Fig. 11.2, the diode polarity indicates that V/V_g must be negative. The steady-state value of R_e is

$$R_e(D) = \frac{2L}{D^2 T_s} \tag{11.27}$$

where D is the quiescent transistor duty cycle. Substitution of Eq. (11.27) into (11.26) leads to

$$\frac{V}{V_g} = -\sqrt{\frac{D^2 T_s R}{2L}} = -\frac{D}{\sqrt{K}} \tag{11.28}$$

with $K = 2L/RT_s$. This equation coincides with the previous steady-state result given in Table 5.2.

Similar arguments apply when the waveforms contain ac components. For example, consider the network of Fig. 11.10, in which the voltages and currents are periodic functions of time. The rms val-

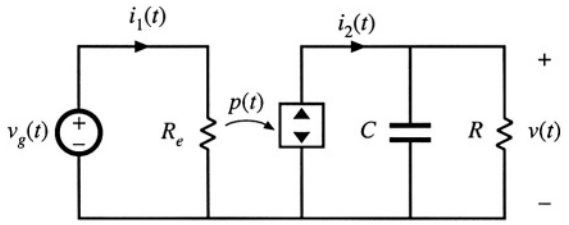

Fig. 11.10 Ac network example containing a loss-free resistor model.

ues of the waveforms can be determined by simply equating the average source and load powers. The average power flowing into the converter input port is

$$P_{av} = \frac{V_{g,rms}^2}{R_e} \tag{11.29}$$

where P_{av} is the average power consumed by the effective resistance R_e. No average power is consumed by capacitor C, and hence the average power P_{av} must flow entirely into the load resistor R:

$$P_{av} = \frac{V_{rms}^2}{R} \tag{11.30}$$

Upon equating Eqs. (11.29) and (11.30), we obtain

$$\frac{V_{rms}}{V_{g,rms}} = \sqrt{\frac{R}{R_e}} \tag{11.31}$$

Thus, the rms terminal voltages obey the same relationship as in the dc case.

Averaged equivalent circuits of the DCM buck, boost, and buck-boost converters, as well as the DCM Ćuk and SEPIC converters, are listed in Fig. 11.11. In each case, the averaged transistor waveforms obey Ohm's law, and are modeled by an effective resistance R_e. The averaged diode waveforms follow a power source characteristic, equal to the power effectively dissipated in R_e. For the buck, boost, and buck-boost converters, R_e is given by

$$R_e = \frac{2L}{d^2 T_s} \tag{11.32}$$

For the Ćuk and SEPIC converters, R_e is given by

$$R_e = \frac{2\left(L_1 \| L_2\right)}{d^2 T_s} \tag{11.33}$$

Here, d is the transistor duty cycle.

Steady-state conditions in the converters of Fig. 11.11 are found by letting the inductors and capacitors become short-circuits and open-circuits, respectively, and then solving the resulting dc circuits with $d(t) = D$. The buck-boost, Ćuk, and SEPIC then reduce to the circuit of Fig. 11.9. The buck and boost converters reduce to the circuits of Fig. 11.12. Equilibrium conversion ratios $M = V/V_g$ of these converters are summarized in Table 11.1, as functions of $R_e(D)$. It can be shown that these converters operate in the discontinuous conduction mode whenever the load current I is less than the critical current I_{crit}:

$$\begin{aligned} I &> I_{crit} \quad \text{for CCM} \\ I &< I_{crit} \quad \text{for DCM} \end{aligned} \tag{11.34}$$

For all of these converters, I_{crit} is given by

$$I_{crit} = \frac{1-D}{D} \frac{V_g}{R_e(D)} \tag{11.35}$$

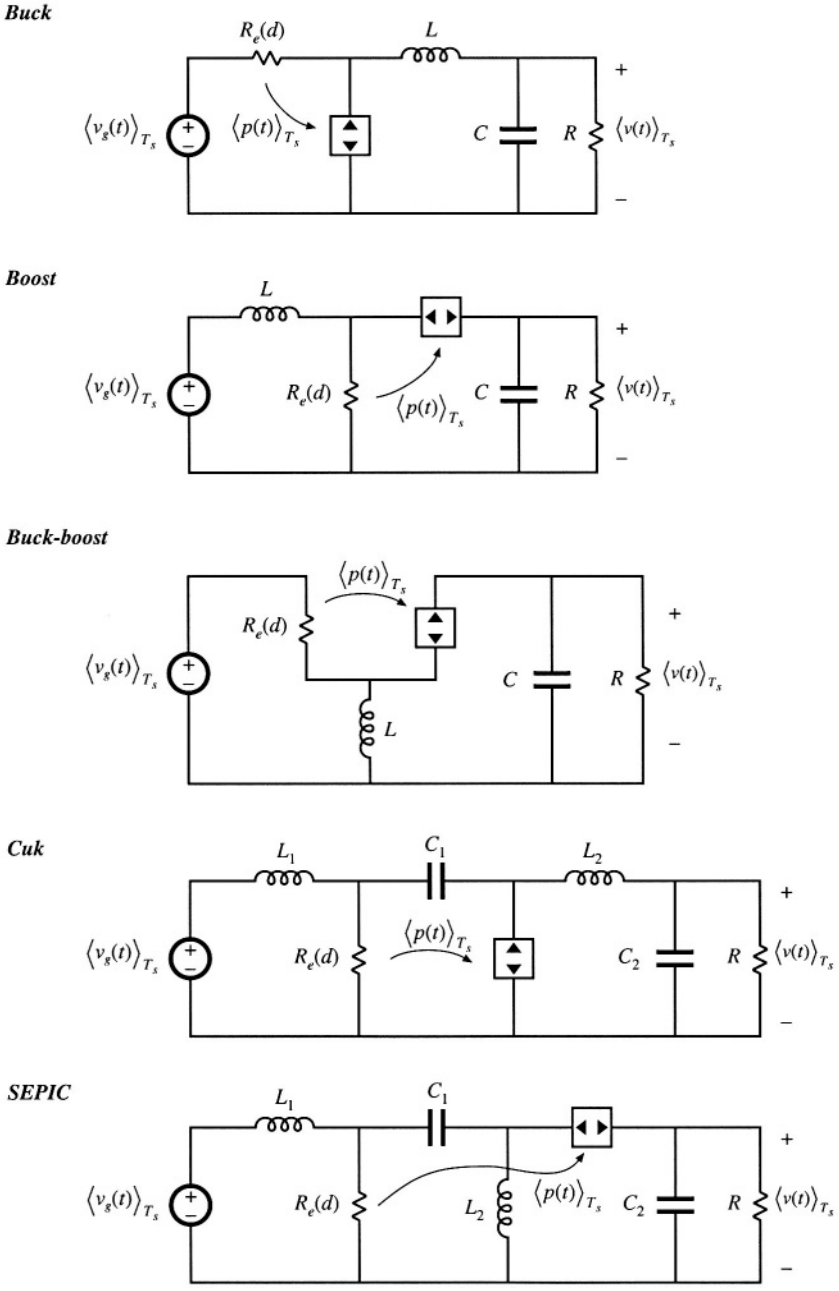

Fig. 11.11 Averaged large-signal equivalent circuits of five basic converters operating in the discontinuous conduction mode.

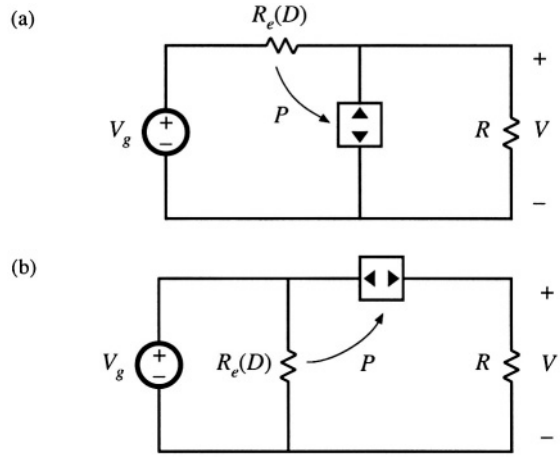

Fig. 11.12 Dc equivalent circuits representing the buck (a) and boost (b) converters operating in DCM.

Table 11.1 CCM and DCM conversion ratios of basic converters

Converter	M, CCM	M, DCM
Buck	D	$\frac{2}{1+\sqrt{1+4R_e/R}}$
Boost	$\frac{1}{1-D}$	$\frac{1+\sqrt{1+4R/R_e}}{2}$
Buck-boost, Ćuk	$\frac{-D}{1-D}$	$-\sqrt{\frac{R}{R_e}}$
SEPIC	$\frac{D}{1-D}$	$\sqrt{\frac{R}{R_e}}$

11.2 SMALL-SIGNAL AC MODELING OF THE DCM SWITCH NETWORK

The next step is construction of a small-signal equivalent circuit model for converters operating in the discontinuous conduction mode. In the large-signal ac equivalent circuits of Fig. 11.11, the averaged switch networks are nonlinear. Hence, construction of a small-signal ac model involves perturbation and linearization of the loss-free resistor network. The signals in the large-signal averaged DCM switch network model of Fig. 11.13(a) are perturbed about a quiescent operating point, as follows:

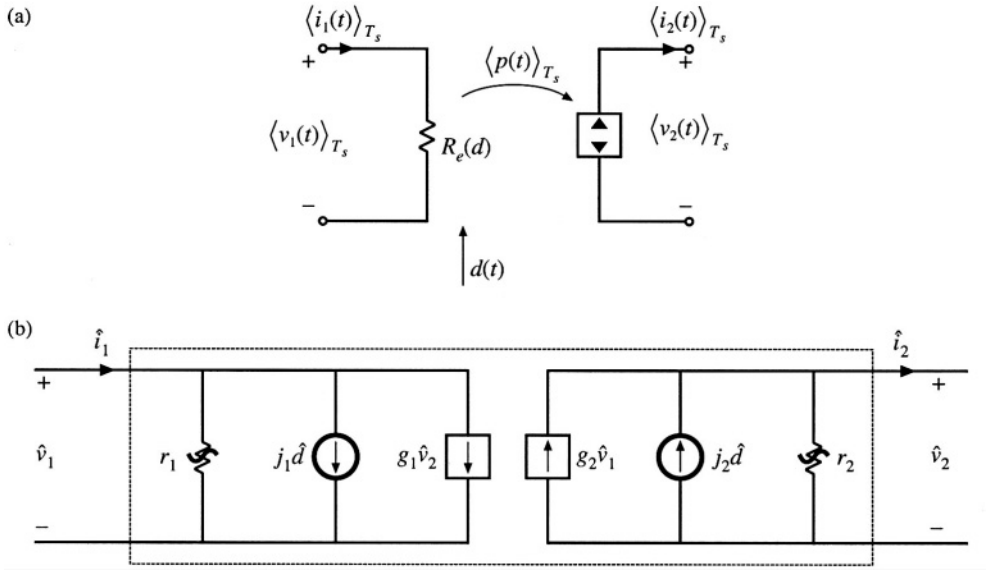

Fig. 11.13 Averaged models of the general two-switch network in a converter operating in DCM: (a) large-signal model, (b) small-signal model.

$$
\begin{aligned}
d(t) &= D + \hat{d}(t) \\
\langle v_1(t)\rangle_{T_s} &= V_1 + \hat{v}_1(t) \\
\langle i_1(t)\rangle_{T_s} &= I_1 + \hat{i}_1(t) \\
\langle v_2(t)\rangle_{T_s} &= V_2 + \hat{v}_2(t) \\
\langle i_2(t)\rangle_{T_s} &= I_2 + \hat{i}_2(t)
\end{aligned}
\tag{11.36}
$$

Here, D is the quiescent value of the transistor duty cycle, V_1 is the quiescent value of the applied average transistor voltage $\langle v_1(t)\rangle_{T_s}$, etc. The quantities $\hat{d}(t)$, $\hat{v}_1(t)$, etc., are small ac variations about the respective quiescent values. It is desired to linearize the average switch network terminal equations (11.15) and (11.16).

Equations (11.15) and (11.16) express the average terminal currents $\langle i_1(t)\rangle_{T_s}$ and $\langle i_2(t)\rangle_{T_s}$ as functions of the transistor duty cycle $d(t) = d_1(t)$ and the average terminal voltages $\langle v_1(t)\rangle_{T_s}$ and $\langle v_2(t)\rangle_{T_s}$. Upon perturbation and linearization of these equations, we will therefore find that $\hat{i}_1(t)$ and $\hat{i}_2(t)$ are expressed as linear functions of $\hat{d}(t)$, $\hat{v}_1(t)$, and $\hat{v}_2(t)$. So the small-signal switch network equations can be written in the following form:

$$
\begin{aligned}
\hat{i}_1 &= \frac{\hat{v}_1}{r_1} + j_1\hat{d} + g_1\hat{v}_2 \\
\hat{i}_2 &= -\frac{\hat{v}_2}{r_2} + j_2\hat{d} + g_2\hat{v}_1
\end{aligned}
\tag{11.37}
$$

These equations describe the two-port equivalent circuit of Fig. 11.13(b).

The parameters r_1, j_1, and g_1 can be found by Taylor expansion of Eq. (11.15), as described in Section 7.2.7. The average transistor current $\langle i_1(t)\rangle_{T_s}$, Eq. (11.15), can be expressed in the following form:

$$\langle i_1(t)\rangle_{T_s} = \frac{\langle v_1(t)\rangle_{T_s}}{R_e\big(d(t)\big)} = f_1\Big(\langle v_1(t)\rangle_{T_s}, \langle v_2(t)\rangle_{T_s}, d(t)\Big) \tag{11.38}$$

Let us expand this expression in a three-dimensional Taylor series, about the quiescent operating point (V_1, V_2, D):

$$\begin{aligned} I_1 + \hat{i}_1(t) = {} & f_1\big(V_1, V_2, D\big) + \hat{v}_1(t)\left.\frac{\partial f_1\big(v_1, V_2, D\big)}{\partial v_1}\right|_{v_1 = V_1} \\ & + \hat{v}_2(t)\left.\frac{\partial f_1\big(V_1, v_2, D\big)}{\partial v_2}\right|_{v_2 = V_2} + \hat{d}(t)\left.\frac{\partial f_1\big(V_1, V_2, d\big)}{\partial d}\right|_{d = D} \\ & + \text{higher-order nonlinear terms} \end{aligned} \tag{11.39}$$

For simplicity of notation, the angle brackets denoting average values are dropped in the above equation. The dc terms on both sides of Eq. (11.39) must be equal:

$$I_1 = f_1\big(V_1, V_2, D\big) = \frac{V_1}{R_e(D)} \tag{11.40}$$

As usual, we linearize the equation by discarding the higher-order nonlinear terms. The remaining first-order linear ac terms on both sides of Eq. (11.39) are equated:

$$\hat{i}_1(t) = \hat{v}_1(t)\,\frac{1}{r_1} + \hat{v}_2(t) g_1 + \hat{d}(t)\, j_1 \tag{11.41}$$

where

$$\frac{1}{r_1} = \left.\frac{\partial f_1\big(v_1, V_2, D\big)}{\partial v_1}\right|_{v_1 = V_1} = \frac{1}{R_e(D)} \tag{11.42}$$

$$g_1 = \left.\frac{\partial f_1\big(V_1, v_2, D\big)}{\partial v_2}\right|_{v_2 = V_2} = 0 \tag{11.43}$$

$$\begin{aligned} j_1 &= \left.\frac{\partial f_1\big(V_1, V_2, d\big)}{\partial d}\right|_{d = D} = -\frac{V_1}{R_e^2(D)}\left.\frac{\partial R_e(d)}{\partial d}\right|_{d = D} \\ &= \frac{2V_1}{DR_e(D)} \end{aligned} \tag{11.44}$$

Thus, the small-signal input resistance r_1 is equal to the effective resistance R_e, evaluated at the quiescent operating point. This term describes how variations in $\langle v_1(t)\rangle_{T_s}$ affect $\langle i_1(t)\rangle_{T_s}$, via $R_e(D)$. The small-signal

parameter g_1 is equal to zero, since the average transistor current $\langle i_1(t)\rangle_{T_s}$ is independent of the average diode voltage $\langle v_2(t)\rangle_{T_s}$. The small-signal gain j_1 describes how duty cycle variations, which affect the value of $R_e(d)$, lead to variations in $\langle i_1(t)\rangle_{T_s}$.

In a similar manner, $\langle i_2(t)\rangle_{T_s}$ from Eq. (11.16) can be expressed as

$$\langle i_2(t)\rangle_{T_s} = \frac{\langle v_1(t)\rangle_{T_s}^2}{R_e\big(d(t)\big)\langle v_2(t)\rangle_{T_s}} = f_2\Big(\langle v_1(t)\rangle_{T_s}, \langle v_2(t)\rangle_{T_s}, d(t)\Big) \tag{11.45}$$

Expansion of the function $f_2(v_1, v_2, d)$ in a three-dimensional Taylor series about the quiescent operating point leads to

$$\begin{aligned} I_2 + \hat{i}_2(t) = {} & f_2\big(V_1, V_2, D\big) + \hat{v}_1(t)\left.\frac{\partial f_2\big(v_1, V_2, D\big)}{\partial v_1}\right|_{v_1 = V_1} \\ & + \hat{v}_2(t)\left.\frac{\partial f_2\big(V_1, v_2, D\big)}{\partial v_2}\right|_{v_2 = V_2} + \hat{d}(t)\left.\frac{\partial f_2\big(V_1, V_2, d\big)}{\partial d}\right|_{d = D} \\ & + \text{higher-order nonlinear terms} \end{aligned} \tag{11.46}$$

By equating the dc terms on both sides of Eq. (11.46), we obtain

$$I_2 = f_2\big(V_1, V_2, D\big) = \frac{V_1^2}{R_e(D)V_2} \tag{11.47}$$

The higher-order nonlinear terms are discarded, leaving the following first-order linear ac terms:

$$\hat{i}_2(t) = \hat{v}_2(t)\left(-\frac{1}{r_2}\right) + \hat{v}_1(t)g_2 + \hat{d}(t)j_2 \tag{11.48}$$

with

$$\frac{1}{r_2} = -\left.\frac{\partial f_2\big(V_1, v_2, D\big)}{\partial v_2}\right|_{v_2 = V_2} = \frac{1}{R} = \frac{1}{M^2 R_e(D)} \tag{11.49}$$

$$g_2 = \left.\frac{\partial f_2\big(v_1, V_2, D\big)}{\partial v_1}\right|_{v_1 = V_1} = \frac{2}{MR_e(D)} \tag{11.50}$$

$$\begin{aligned} j_2 &= \left.\frac{\partial f_2\big(V_1, V_2, d\big)}{\partial d}\right|_{d = D} = -\frac{V_1^2}{R_e^2(D)V_2}\left.\frac{\partial R_e(d)}{\partial d}\right|_{d = D} \\ &= \frac{2V_1}{DMR_e(D)} \end{aligned} \tag{11.51}$$

The output resistance r_2 describes how variations in $\langle v_2(t)\rangle_{T_s}$ influence $\langle i_2(t)\rangle_{T_s}$. As illustrated in Fig. 11.14,

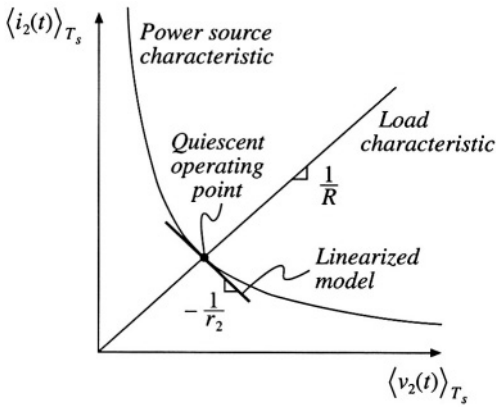

Fig. 11.14 The small-signal output resistance r_2 is determined by the slope of the power source characteristic at the quiescent operating point.

Table 11.2 Small-signal DCM switch model parameters

Switch network	g_1	j_1	r_1	g_2	j_2	r_2
General two-switch, Fig. 11.7(a)	0	$\frac{2V_1}{DR_e}$	R_e	$\frac{2}{MR_e}$	$\frac{2V_1}{DMR_e}$	M^2R_e
Buck, Fig. 11.16(a)	$\frac{1}{R_e}$	$\frac{2(1-M)V_1}{DR_e}$	R_e	$\frac{2-M}{MR_e}$	$\frac{2(1-M)V_1}{DMR_e}$	M^2R_e
Boost, Fig. 11.16(b)	$\frac{1}{(M-1)^2R_e}$	$\frac{2MV_1}{D(M-1)R_e}$	$\frac{(M-1)^2}{M^2}R_e$	$\frac{2M-1}{(M-1)^2R_e}$	$\frac{2V_1}{D(M-1)R_e}$	$(M-1)^2R_e$

r_2 is determined by the slope of the power source characteristic, evaluated at the quiescent operating point. For a linear resistive load, $r_2 = R$. For any type of load, it is true that $r_2 = M^2R_e(D)$. The parameters j_2 and g_2 describe how variations in the duty cycle $d(t)$ and in the average transistor voltage $\langle v_1(t)\rangle_{T_s}$ (which influence the average power $\langle p(t)\rangle_{T_s}$) lead to variations in the average diode current $\langle i_2(t)\rangle_{T_s}$. Values of the small-signal parameters in the DCM switch model of Fig. 11.13(b) are summarized in the top row of Table 11.2.

A small-signal model of the DCM buck-boost converter is obtained by replacing the transistor and diode of the converter with the switch model of Fig. 11.13(b). The result is illustrated in Fig. 11.15. This equivalent circuit can now be solved using conventional linear circuit analysis techniques, to determine the transfer functions and other small-signal quantities of interest.

The same small-signal switch model can be employed to model other DCM converters, by simply replacing the transistor and diode with ports 1 and 2, respectively, of the two-port model of Fig. 11.13(b). An alternative approach, which yields more convenient results in the analysis of the buck and boost converters, is to define the switch network as illustrated in Figs. 11.16(a) and 11.16(b), respectively. These switch networks can also be modeled using the two-port small-signal equivalent circuit of Fig. 11.16(c); however, new expressions for the parameters r_1, j_1, g_1, etc., must be derived. These expressions are again found by linearizing the equations of the averaged switch network terminal currents.

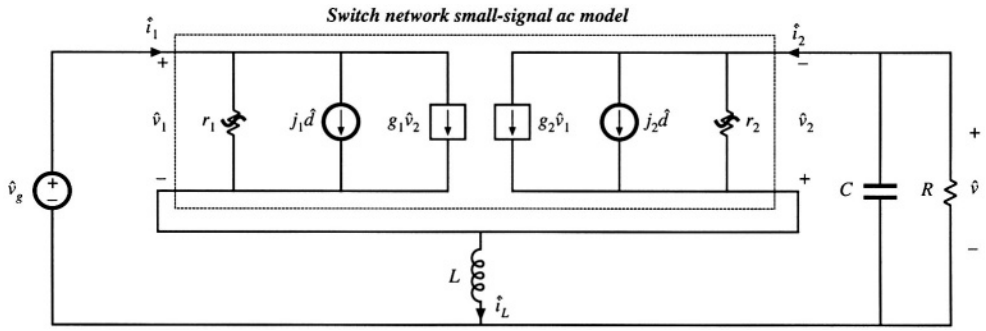

Fig. 11.15 Small-signal ac model of the DCM buck-boost converter obtained by insertion of the switch network two-port small-signal model into the original converter circuit.

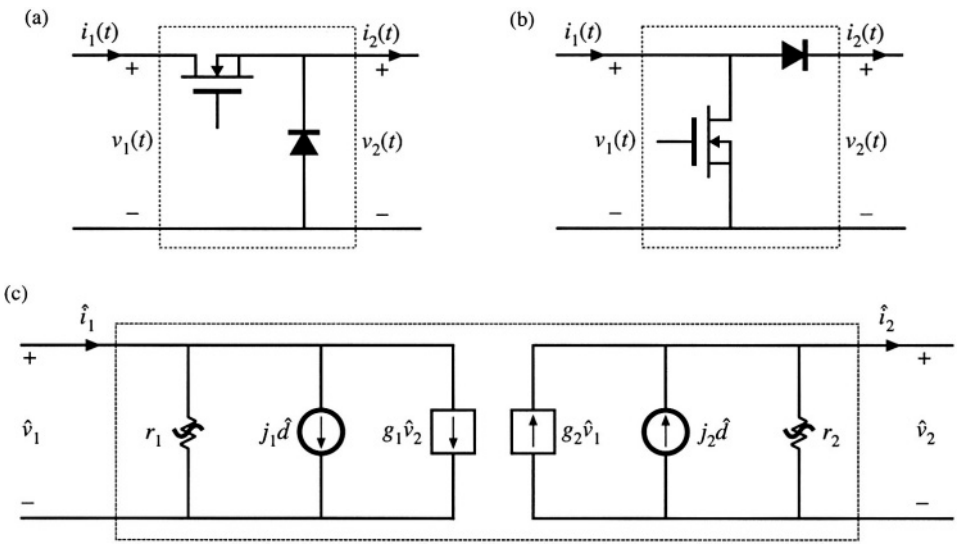

Fig. 11.16 A convenient way to model the switch networks of DCM buck and boost converters: (a) defined terminal quantities of the DCM buck switch network, (b) defined terminal quantities of the boost switch network, (c) two-port small-signal ac model. The model parameters are given in Table 11.2.

Table 11.2 lists the small-signal parameters for the buck switch network of Fig. 11.16(a) (middle row) and for the boost switch network of Fig. 11.16(b) (bottom row). Insertion of the small-signal two-port model into the DCM buck and boost converters leads to the equivalent circuits of Fig. 11.17.

The small-signal equivalent circuit models of Fig. 11.15 and Fig. 11.17 contain two dynamic elements: capacitor C and inductor L. Control-to-output transfer functions obtained by solving these equivalent circuit models have two poles. It has been shown [2-6] that one of the poles, due to the capacitor C, appears at a low frequency, while the other pole (and a RHP zero in the case of boost and buck-

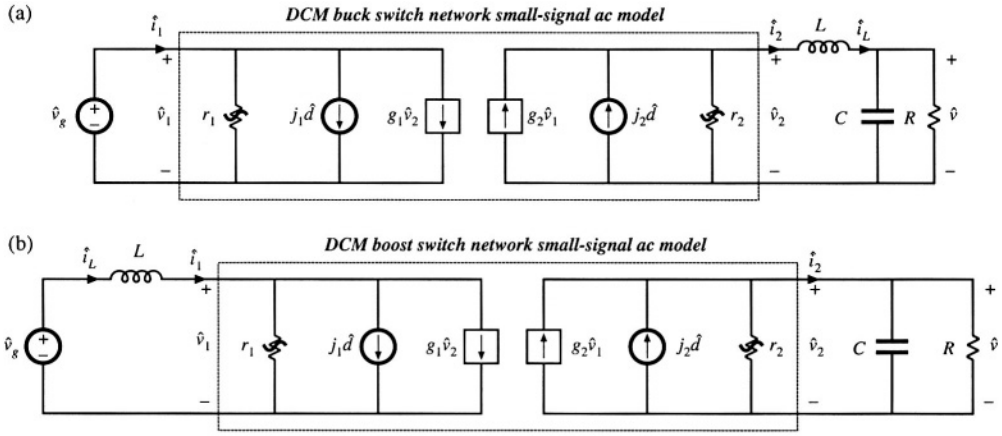

Fig. 11.17 Small-signal ac models of (a) the DCM buck converter, and (b) the DCM boost converter, obtained by replacing the switch networks defined in Fig. 11.16(a) and (b) with the small-signal switch model of Fig. 11.16(c).

boost converters) due to the inductor L, occurs at much higher frequency, close to the converter switching frequency. Therefore, in practice, the DCM buck, boost, and buck-boost converters exhibit essentially single-pole transfer functions, which are negligibly influenced by the inductor dynamics.

The small-signal equivalent circuit models have been derived in this section from the large-signal averaged switch network equations (11.15) and (11.16). These equations are based on Eq. (11.11), which states that the average inductor voltage, and therefore its small-signal ac voltage, is zero. This contradicts predictions of the resulting small-signal models in Figs. 11.15 and 11.17. As a result, we expect that the models derived in this section can be used to predict low-frequency dynamics, while predictions of the high-frequency dynamics due to the inductor L are of questionable validity. Equivalent circuit models that give more accurate predictions of high-frequency dynamics of DCM converters are discussed in Section 11.3.

A simple approximate way to determine the low-frequency small-signal transfer functions of the buck, boost, and buck-boost converters is to let the inductance L tend to zero. If L is shorted in the equivalent circuits of Figs. 11.15 and 11.17, the model in all three cases reduces to Fig. 11.18. This cir-

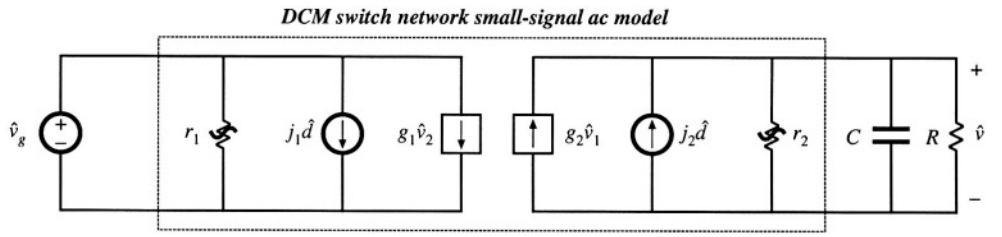

Fig. 11.18 Low-frequency ac model obtained by letting L approach zero. The buck, boost, or buck-boost converters can be modeled, by employing the appropriate parameters from Table 11.2.

cuit is relatively easy to solve.

The control-to-output transfer function $G_{vd}(s)$ is found by letting $\hat{v}_g = 0$ in Fig. 11.18. Solution for $\hat{v}$ then leads to

$$G_{vd}(s) = \left.\frac{\hat{v}}{\hat{d}}\right|_{\hat{v}_g = 0} = \frac{G_{d0}}{1 + \frac{s}{\omega_p}} \tag{11.52}$$

with

$$\begin{aligned} G_{d0} &= j_2\left(R \| r_2\right) \\ \omega_p &= \frac{1}{\left(R \| r_2\right) C} \end{aligned} \tag{11.53}$$

The line-to-output transfer function $G_{vg}(s)$ is found by letting $\hat{d} = 0$ in Fig. 11.18. One then obtains

$$G_{vg}(s) = \left.\frac{\hat{v}}{\hat{v}_g}\right|_{\hat{d} = 0} = \frac{G_{g0}}{1 + \frac{s}{\omega_p}} \tag{11.54}$$

with

$$G_{g0} = g_2\left(R \| r_2\right) = M \tag{11.55}$$

Expressions for G_{d0}, G_{g0}, and ω_p are listed in Table 11.3, for the DCM buck, boost, and buck-boost converters with resistive loads [12,13].

The ac modeling approach described in this section is both general and useful. The transistor and diode of a DCM converter can be simply replaced by the two-port network of Fig. 11.13(b), leading to the small-signal ac model. Alternatively, the switch network can be defined as in Fig. 11.16(a) or 11.16(b), and then modeled by the same two-port network, Fig. 11.16(c). The small-signal converter model can then be solved via conventional circuit analysis techniques, to obtain the small-signal transfer functions of the converter.

Table 11.3 Salient features of DCM converter small-signal transfer functions

Converter	G_{d0}	G_{g0}	ω_p
Buck	$\frac{2V}{D}\frac{1-M}{2-M}$	M	$\frac{2-M}{(1-M)RC}$
Boost	$\frac{2V}{D}\frac{M-1}{2M-1}$	M	$\frac{2M-1}{(M-1)RC}$
Buck–boost	$\frac{V}{D}$	M	$\frac{2}{RC}$

11.2.1 Example: Control-to-Output Frequency Response of a DCM Boost Converter

As a simple numerical example, let us find the small-signal control-to-output transfer function of a DCM boost converter having the following element and parameter values:

$$\begin{aligned} R &= 12\ \Omega \\ L &= 5\ \mu\text{H} \\ C &= 470\ \mu\text{F} \\ f_s &= 100\ \text{kHz} \end{aligned} \tag{11.56}$$

The output voltage is regulated to be $V = 36$ V. It is desired to determine $G_{vd}(s)$ at the operating point where the load current is $I = 3$ A and the dc input voltage is $V_g = 24$ V.

The effective resistance $R_e(D)$ is found by solution of the dc equivalent circuit of Fig. 11.12(b). Since the load current I and the input and output voltages V and V_g are known, the power source value P is

$$P = I\left(V - V_g\right) = \left(3\ \text{A}\right)\left(36\ \text{V} - 24\ \text{V}\right) = 36\ \text{W} \tag{11.57}$$

The effective resistance is therefore

$$R_e = \frac{V_g^2}{P} = \frac{(24\ \text{V})^2}{36\ \text{W}} = 16\ \Omega \tag{11.58}$$

The steady-state duty cycle D can now be found using Eq. (11.32):

$$D = \sqrt{\frac{2L}{R_e T_s}} = \sqrt{\frac{2(5\ \mu\text{H})}{(16\ \Omega)(10\ \mu\text{s})}} = 0.25 \tag{11.59}$$

The expressions given in Table 11.3 for G_{d0} and ω_p of the boost converter can now be evaluated:

$$\begin{aligned} G_{d0} &= \frac{2V}{D}\,\frac{M-1}{2M-1} = \frac{2(36\ \text{V})}{(0.25)}\,\frac{\left(\dfrac{(36\ \text{V})}{(24\ \text{V})} - 1\right)}{\left(2\dfrac{(36\ \text{V})}{(24\ \text{V})} - 1\right)} = 72\ \text{V} \Rightarrow 37\ \text{dBV} \\ f_p &= \frac{\omega_p}{2\pi} = \frac{2M-1}{2\pi(M-1)RC} = \frac{\left(2\dfrac{(36\ \text{V})}{(24\ \text{V})} - 1\right)}{2\pi\left(\dfrac{(36\ \text{V})}{(24\ \text{V})} - 1\right)(12\ \Omega)(470\ \mu\text{F})} = 112\ \text{Hz} \end{aligned} \tag{11.60}$$

A Bode diagram of the control-to-output transfer function is constructed in Fig. 11.19. The solid lines illustrate the magnitude and phase predicted by the approximate single-pole model of Fig. 11.18. The dashed lines are the predictions of the more accurate model discussed in Section 11.3, which include a second pole at $f_2 = 64$ kHz and a RHP zero at $f_z = 127$ kHz, arising from the inductor dynamics. Since the switching frequency is 100 kHz, the accuracy of the model at these frequencies cannot be guaranteed. Nonetheless, in practice, the lagging phase asymptotes arising from the inductor dynamics can be

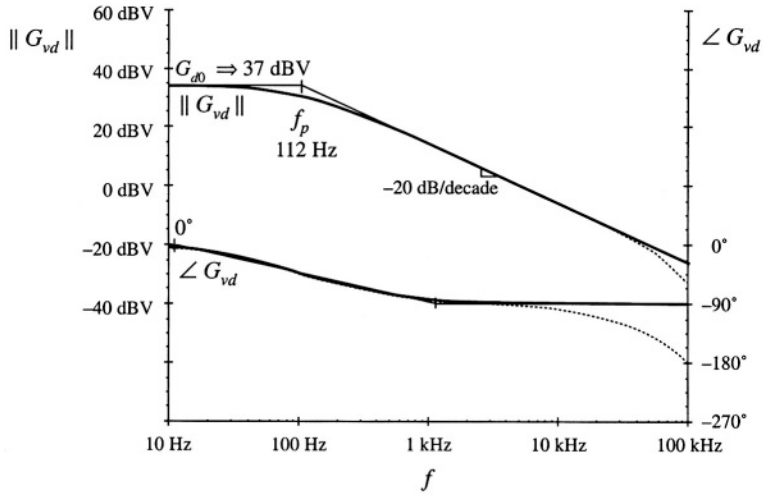

Fig. 11.19 Magnitude and phase of the control-to-output transfer function, DCM boost example. Solid lines: function and its asymptotes, approximate single-pole response predicted by the model of Fig. 11.18. Dashed lines: more accurate response that includes high-frequency inductor dynamics.

observed beginning at $f_2/10 = 6.4$ kHz.

11.2.2 Example: Control-to-Output Frequency Responses of a CCM/DCM SEPIC

As another example, consider the SEPIC of Fig. 11.20. According to Eq. (11.34), this converter operates in CCM if

$$\frac{V}{R} > \frac{1-D}{D}\frac{V_g}{R_e(D)} \tag{11.61}$$

where $R_e(D)$ is given by Eq. (11.33). Upon neglecting losses in the converter, one finds that the CCM conversion ratio is

$$\frac{V}{V_g} \approx \frac{D}{1-D} \tag{11.62}$$

When Eqs. (11.33) and (11.62) are substituted into Eq. (11.61), the condition for operation in CCM becomes:

$$R < \frac{2\left(L_1 \| L_2\right)}{(1-D)^2 T_s} = 46\ \Omega \tag{11.63}$$

The converter control-to-output frequency responses are generated using Spice ac simulations. Details of

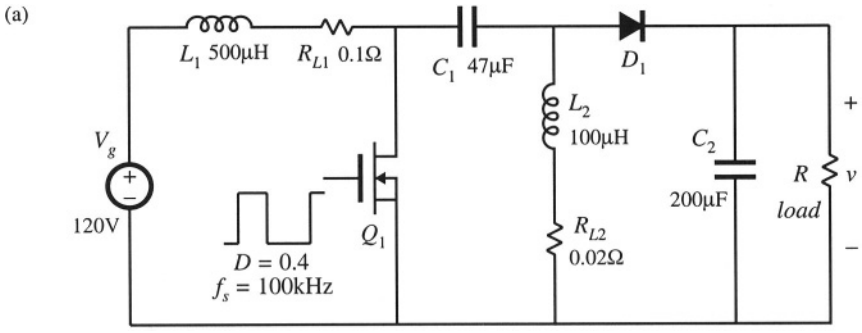

Fig. 11.20 SEPIC example.

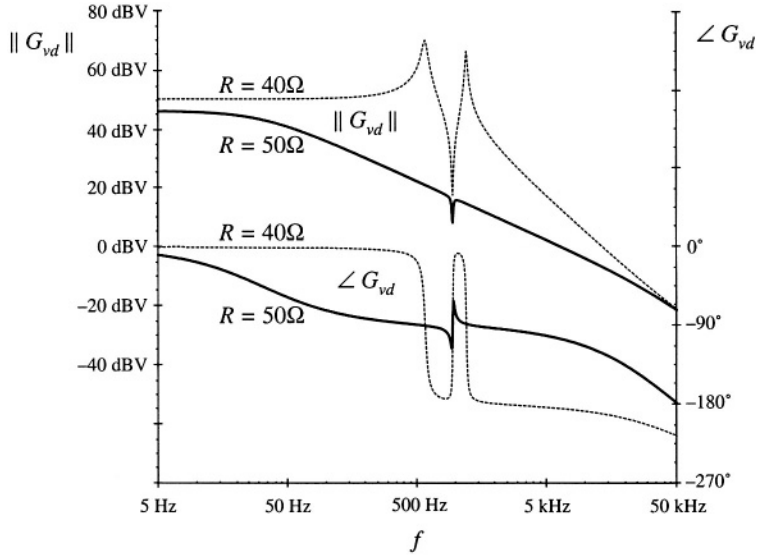

Fig. 11.21 Magnitude and phase of the control-to-output transfer function obtained by simulation of the SEPIC example shown in Fig. 11.20, for two values of the load resistance: $R = 50\Omega$ when the converter operates in DCM (solid lines), and $R = 40\Omega$ for which the converter operates in CCM (dashed lines).

the simulation setup are described in Appendix B, Section B.2.1. Figure 11.21 shows magnitude and phase responses of the control-to-output transfer function obtained for two different values of the load resistance: $R = 40\ \Omega$, for which the converter operates in CCM, and $R = 50\ \Omega$, for which the converter operates in DCM. For these two operating points, the quiescent (dc) voltages and currents in the circuit are nearly the same. Nevertheless, the frequency responses are qualitatively very different in the two operating modes. In CCM, the converter exhibits a fourth-order response with two pairs of high-Q complex-conjugate poles and a pair of complex-conjugate zeros. Another RHP (right-half plane) zero can be observed at frequencies approaching 50 kHz. In DCM, there is a dominant low-frequency pole followed

by a pair of complex-conjugate poles and a pair of complex-conjugate zeros. The frequencies of the complex poles and zeros are very close in value. A high-frequency pole and a RHP zero contribute additional phase lag at higher frequencies.

11.3 HIGH-FREQUENCY DYNAMICS OF CONVERTERS IN DCM

As discussed in Section 11.2, transfer functions of converters operating in discontinuous conduction mode exhibit a dominant low-frequency pole. A pole and possibly a zero caused by inductor dynamics, are pushed to high frequencies. To correctly model the high-frequency dynamics of DCM converters, one must account for the fact that the ac voltage across the inductor is not zero. Equation (11.12) is employed in Section 11.1 to greatly simplify the equations of the DCM averaged switch model. Although this model gives good results at low frequencies, it cannot accurately predict high frequency inductor dynamics because it implies that the ac inductor voltage is zero.

A more accurate approach is employed in this section. The subinterval length d_2 is found by averaging the inductor current waveform $i_L(t)$ of Fig. 11.3 [4-6]:

$$\left\langle i_L(t)\right\rangle_{T_s} = \frac{1}{2} i_{pk}\left(d(t) + d_2(t)\right) = \frac{d(t)\left(d(t) + d_2(t)\right)T_s}{2L}\left\langle v_g(t)\right\rangle_{T_s} \tag{11.64}$$

Solution for $d_2(t)$ yields:

$$d_2(t) = \frac{2L\left\langle i_L(t)\right\rangle_{T_s}}{d(t)T_s\left\langle v_g(t)\right\rangle_{T_s}} - d(t) = \left(\frac{R_e(d)\left\langle i_L(t)\right\rangle_{T_s}}{\left\langle v_g(t)\right\rangle_{T_s}} - 1\right) d(t) \tag{11.65}$$

Equation (11.65), together with Eqs. (11.3), (11.4), (11.7), and (11.10), constitutes a large-signal averaged model in DCM that can be used to investigate steady-state behavior, as well as low-frequency and high-frequency dynamics. Unfortunately, the model equations are more involved, and do not allow elimination of all converter voltages and currents in terms of the switch network average terminal waveforms.

Let us use this model to find predictions for the high-frequency pole caused by the inductor dynamics of DCM converters. Consider the buck-boost converter of Fig. 11.2 having the DCM waveforms shown in Fig. 11.3. The average transistor voltage $\langle v_1(t)\rangle_{T_s}$ and the average diode current $\langle i_2(t)\rangle_{T_s}$ are selected as the switch network dependent variables. Substitution of Eq. (11.65) into Eq. (11.3) yields

$$\left\langle v_1(t)\right\rangle_{T_s} = \left(1 - d(t)\right)\left\langle v_g(t)\right\rangle_{T_s} + d(t)\left\langle v(t)\right\rangle_{T_s} - \frac{R_e(d)\left\langle i_L(t)\right\rangle_{T_s}\left\langle v(t)\right\rangle_{T_s} d(t)}{\left\langle v_g(t)\right\rangle_{T_s}} \tag{11.66}$$

The averaged switch voltage $\langle v_1(t)\rangle_{T_s}$ in Eq. (11.66) is a nonlinear function of the switch duty cycle, the average inductor current, and the average input and output voltages:

$$\left\langle v_1(t)\right\rangle_{T_s} = \gamma_1\left(\left\langle v_g(t)\right\rangle_{T_s}, \left\langle v(t)\right\rangle_{T_s}, \left\langle i_L(t)\right\rangle_{T_s}, d(t)\right) \tag{11.67}$$

A small-signal ac model can be obtained by Taylor expansion of Eq. (11.67). The small-signal ac component $\hat{v}_1$ of the average switch voltage can be found as:

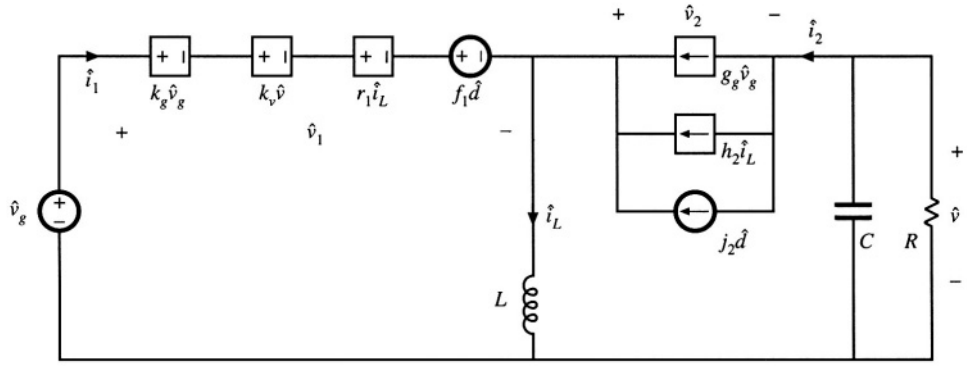

Fig. 11.22 A small-signal ac model of the DCM buck-boost converter.

$$\hat{v}_1(t) = \hat{v}_g(t)k_g + \hat{v}(t)k_v + \hat{i}_L r_1 + \hat{d}(t)f_1 \tag{11.68}$$

where the small-signal model parameters k_g, k_v, r_1, and f_1 are computed as partial derivatives of γ_1 evaluated at the quiescent operating point. In particular,

$$r_1 \equiv \left.\frac{\partial \gamma_1\left(V_g, V, i_L, D\right)}{\partial i_L}\right|_{i_L = I_L} = -\frac{V}{V_g}R_e D \tag{11.69}$$

Substitution of Eq. (11.65) into Eq. (11.10) yields

$$\left\langle i_2(t)\right\rangle_{T_s} = \left\langle i_L(t)\right\rangle_{T_s} - \frac{\left\langle v_g(t)\right\rangle_{T_s}}{R_e} = \gamma_2\left(\left\langle v_g(t)\right\rangle_{T_s}, \left\langle i_L(t)\right\rangle_{T_s}, d(t)\right) \tag{11.70}$$

The small-signal ac component $\hat{i}_2$ of the average diode current can be found as:

$$\hat{i}_2(t) = \hat{v}_g(t)g_g + \hat{i}_L h_2 + \hat{d}(t)j_2 \tag{11.71}$$

where the small-signal model parameters g_g, h_2, and j_2 are computed as partial derivatives of γ_2 evaluated at the quiescent operating point. Figure 11.22 shows the small-signal ac model of the buck-boost converter, where the transistor and the diode switch are replaced by the sources specified by Eqs. (11.68) and (11.71), respectively. It can be shown that this model predicts essentially the same low-frequency dynamics as the model derived in Section 11.2.

To find the control-to-output transfer function, we set $\hat{v}_g = 0$. At high frequencies, the small-signal ac component of the capacitor voltage is very small, $\hat{v} \approx 0$. Therefore, the contribution of the dependent source $k_v\hat{v}$ can be neglected at high frequencies. Then, from the equivalent circuit model of Fig. 11.22, we have

$$sL\hat{i}_L + r_1\hat{i}_L + f_1\hat{d} = 0 \tag{11.72}$$

Equation (11.72) can be solved for the control-to-inductor current transfer function at high frequencies:

$$\frac{\hat{i}_L}{\hat{d}} = -\frac{f_1}{r_1}\frac{1}{1+\frac{s}{\omega_2}} \tag{11.73}$$

where the pole frequency f_2 is given by

$$f_2 = \frac{\omega_2}{2\pi} = \frac{r_1}{2\pi L} \tag{11.74}$$

To simplify the expression for the pole frequency f_2, we use the steady-state relationship that follows from Eq. (11.12):

$$-\frac{V}{V_g} = \frac{D}{D_2} \tag{11.75}$$

Also, recall that the steady-state equivalent resistance $R_e(D)$ can be written as

$$R_e = \frac{2Lf_s}{D^2} \tag{11.76}$$

where f_s is the switching frequency. Upon substitution of Eqs. (11.69), (11.75) and (11.76) into Eq. (11.74) we get:

$$f_2 = \frac{f_s}{\pi D_2} \tag{11.77}$$

This is an expression for the frequency f_2 of the high-frequency pole that is caused by the inductor dynamics of the DCM buck-boost converter. It can be shown that Eq. (11.77) is a general result for the high-frequency pole, valid for all basic converters operating in DCM. Since $0 < D_2 < 1$, Eq. (11.77) implies that the high-frequency pole is always greater than approximately one third of the switching frequency.

Table 11.4 summarizes the expressions for the high-frequency pole ω_2 and the RHP zero ω_z caused by the inductor dynamics in control-to-output transfer functions $G_{vd}(s)$ of basic DCM converters [6]. The high-frequency pole and the RHP zero occur at frequencies close to or exceeding the switching frequency f_s. This is why, in practice, the high-frequency inductor dynamics can usually be neglected.

Table 11.4 High-frequency pole and RHP zero of the DCM converter control-to-output transfer function $G_{vd}(s)$

Converter	High-frequency pole ω_2	RHP zero ω_z
Buck	$\frac{2Mf_s}{D(1-M)}$	none
Boost	$\frac{2(M-1)f_s}{D}$	$\frac{2f_s}{D}$
Buck–boost	$\frac{2\lvert M\rvert f_s}{D}$	$\frac{2f_s}{D}$

11.4 SUMMARY OF KEY POINTS

1. In the discontinuous conduction mode, the average transistor voltage and current are proportional, and hence obey Ohm's law. An averaged equivalent circuit can be obtained by replacing the transistor with an effective resistor $R_e(d)$. The average diode voltage and current obey a power source characteristic, with power equal to the power effectively dissipated by R_e. In the averaged equivalent circuit, the diode is replaced with a dependent power source.
2. The two-port lossless network consisting of an effective resistor and power source, which results from averaging the transistor and diode waveforms of DCM converters, is called a loss-free resistor. This network models the basic power-processing functions of DCM converters, much in the same way that the ideal dc transformer models the basic functions of CCM converters.
3. The large-signal averaged model can be solved under equilibrium conditions to determine the quiescent values of the converter currents and voltages. Average power arguments can often be used.
4. A small-signal ac model for the DCM switch network can be derived by perturbing and linearizing the loss-free resistor network. The result has the form of a two-port *y*-parameter model. The model describes the small-signal variations in the transistor and diode currents, as functions of variations in the duty cycle and in the transistor and diode ac voltage variations.
5. To simplify the ac analysis of the DCM buck and boost converters, it is convenient to define two other forms of the small-signal switch model, corresponding to the switch networks of Figs. 11.16(a) and 11.16(b). These models are also *y*-parameter two-port models, but have different parameter values.
6. The inductor dynamics of the DCM buck, boost, and buck-boost converters occur at high frequency, above or just below the switching frequency. Hence, in most cases the high frequency inductor dynamics can be ignored. In the small-signal ac model, the inductance L is set to zero, and the remaining model is solved relatively easily for the low-frequency converter dynamics. The DCM buck, boost, and buck-boost converters exhibit transfer functions containing essentially a single low-frequency dominant pole.
7. To obtain a more accurate model of the inductor dynamics in DCM, it is necessary to write the equations of the averaged inductor waveforms in a way that does not assume that the average inductor voltage is zero.

REFERENCES

[1] V. VORPERIAN, R. TYMERSKI, and F. C. LEE, "Equivalent Circuit Models for Resonant and PWM Switches," *IEEE Transactions on Power Electronics,* Vol. 4, No. 2, pp. 205-214, April 1989.

[2] V. VORPERIAN, "Simplified Analysis of PWM Converters Using the Model of the PWM Switch," parts I and II, *IEEE Transactions on Aerospace and Electronic Systems,* Vol. 26, No. 3, May 1990, pp. 490-505.

[3] D. MAKSIMOVIĆ and S. ĆUK, "A Unified Analysis of PWM Converters in Discontinuous Modes," *IEEE Transactions on Power Electronics,* Vol. 6, No. 3, pp. 476-490, July 1991.

[4] J. SUN, D. M. MITCHELL, M. GREUEL, P. T. KREIN, and R. M. BASS, "Averaged Modelling of PWM Converters in Discontinuous Conduction Mode: a Reexamination," *IEEE Power Electronics Specialists Conference,* 1998 Record, pp. 615-622, June 1998.

[5] S. BEN-YAAKOV and D. ADAR, "Average Models as Tools for Studying Dynamics of Switch Mode DC–DC Converters," *IEEE Power Electronics Specialists Conference,* 1994 Record, pp. 1369-1376, June 1994.

[6] J. SUN, D. M. MITCHELL, M. GREUEL, P. T. KREIN, and R. M. BASS, "Average Models for PWM Converters in Discontinuous Conduction Mode," *Proceedings of the 1998 International High Frequency Power Coversion Conference* (HFPC'98), pp. 61-72, November 1998.

[7] A. WITULSKI and R. ERICKSON, "Extension of State-Space Averaging to Resonant Switches —and Beyond," *IEEE Transactions on Power Electronics,* Vol. 5, No. 1, pp. 98-109, January 1990.

[8] S. FREELAND and R. D. MIDDLEBROOK, "A Unified Analysis of Converters with Resonant Switches," *IEEE Power Electronics Specialists Conference,* 1987 Record, pp. 20-30, June 1987.

[9] S. SINGER, "Realization of Loss-Free Resistive Elements," *IEEE Transactions on Circuits and Systems,* Vol. CAS-36, No. 12, January 1990.

[10] S. SINGER and R.W. ERICKSON, "Power-Source Element and Its Properties," *IEE Proceedings—Circuits Devices and Systems,* Vol. 141, No. 3, pp. 220-226, June 1994.

[11] S. SINGER and R. ERICKSON, "Canonical Modeling of Power Processing Circuits Based on the POPI Concept," *IEEE Transactions on Power Electronics,* Vol. 7, No. 1, January 1992.

[12] S. ĆUK and R. D. MIDDLEBROOK, "A General Unified Approach to Modeling Switching Dc-to-Dc Converters in Discontinuous Conduction Mode," *IEEE Power Electronics Specialists Conference,* 1977 Record, pp. 36-57.

[13] S. ĆUK, "Modeling, Analysis, and Design of Switching Converters," Ph.D. Thesis, California Institute of Technology, November 1976.

PROBLEMS

11.1 Averaged switch modeling of a flyback converter. The converter of Fig. 11.23 operates in the discontinuous conduction mode. The two-winding inductor has a 1:n turns ratio and negligible leakage inductance, and can be modeled as an ideal transformer in parallel with primary-side magnetizing inductance L_p.

(a) Sketch the transistor and diode voltage and current waveforms, and derive expressions for their average values.

(b) Sketch an averaged model for the converter that includes a loss-free resistor network, and give an expression for $R_e(d)$.

(c) Solve your model to determine the voltage ratio V/V_g in the discontinuous conduction mode.

(d) Over what range of load current I is your answer of part (c) valid? Express the DCM boundary in the form $I < I_{crit}(D, R_e, V_g, n)$.

(e) Derive an expression for the small-signal control-to-output transfer function $G_{vd}(s)$. You may neglect inductor dynamics.

11.2 Averaged switch modeling of a nonisolated Watkins-Johnson converter. The converter of Fig. 11.24 operates in the discontinuous conduction mode. The two-winding inductor has a 1:1 turns ratio and negligible leakage inductance, and can be modeled as an ideal transformer in parallel with magnetizing inductance L.

(a) Sketch the transistor and diode voltage and current waveforms, and derive expressions for their average values.

(b) Sketch an averaged model for the converter that includes a loss-free resistor network, and give an expression for $R_e(d)$.

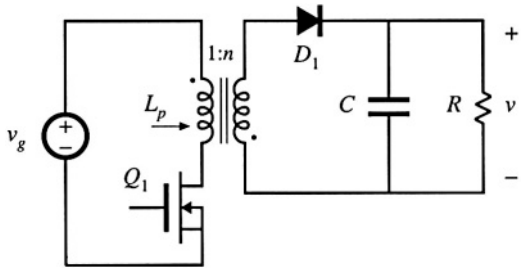

Fig. 11.23 Flyback converter, Problem 11.1.

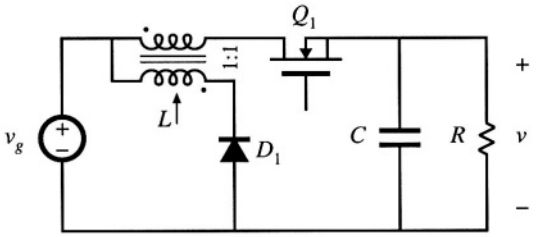

Fig. 11.24 Watkins-Johnson converter, Problem 11.2.

(c) Solve your model to determine the converter conversion ratio $M(D) = V/V_g$ in the discontinuous conduction mode. Over what range of load currents is your expression valid?

11.3 Sketch the steady-state output characteristics of the buck-boost converter: plot the output voltage V vs. the load current I, for several values of duty cycle D. Include both CCM and DCM operation, and clearly label the boundary between modes.

11.4 In the network of Fig. 11.25, the power source waveform $p(t)$ is given by

$$p(t) = 1000 \cos^2 377t$$

The circuit operates in steady state. Determine the rms resistor voltage $V_{R,rms}$.

11.5 Verify the expressions for G_{d0} and ω_p given in Table 11.3.

11.6 A certain buck converter operates with an input voltage of $V_g = 28$ V and an output voltage of $V = 15$ V. The load resistance is $R = 10\Omega$. Other element and parameter values are: $L = 8\mu H$, $C = 220\mu F$, $f_s = 150$kHz.

(a) Determine the value of R_e.

(b) Determine the quiescent duty cycle D.

(c) Sketch a Bode plot of the control-to-output transfer function $G_{vd}(s)$. Label the values of all salient features. You may neglect inductor dynamics.

11.7 Using the approach of Section 11.3, determine the control-to-output transfer function $G_{vd}(s)$ of a boost converter. Do not make the approximation $L \approx 0$.

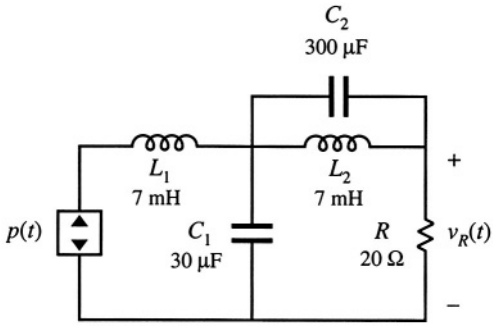

Fig. 11.25 Network with a power source, Problem 11.4.

(a) Derive analytical expressions for the dc gain G_{d0} and the RHP zero frequency ω_z, as functions of M, R_e, D, V_g, L, C, and R.

(b) With the assumption that C is sufficiently large and that L is sufficiently small, the poles of $G_{vd}(s)$ can be factored using the low-Q approximation. Do so, and express the two poles as functions of M, D, L, C, and R. Show that the low-frequency pole matches the expression in Table 11.3, and that the high-frequency pole is given by the expression in Table 11.4.